Highlights

Inter-regional Unit Commitment and PV Scheduling Considering Frequency Constraints

Hongxing Ye, Cheng Zhou, Nan Wei, Siwei Liu, Dong Xing

- This work presents an inter-regional unit commitment with semi-dispatchable PV generation.
- HVDC tie-line frequency support is considered based on multi-machine system frequency response.
- A solution approach Successive Constraint Generation is proposed to address the nonlinear frequency limit constraints.
- The proposed approach helps increase the frequency-secure disturbance for PV generation.

Inter-regional Unit Commitment and PV Scheduling Considering Frequency Constraints

Hongxing Ye[a], Cheng Zhou[a], Nan Wei[b], Siwei Liu[b], Dong Xing[b]

[a]*Xi'an Jiaotong University, , Xi'an, 710049, Shaanxi, China*
[b]*State Grid Economic and Tech. Research Inst. Co. Ltd, , Beijing, 102209, Beijing, China*

Abstract

Unit commitment problem considering renewable uncertainty has received a lot of attention in recent years. The high-level penetration of renewable lowers the system inertia, posing challenges in frequency stability. This work proposes a unit commitment model considering frequency limits. High Voltage Direct Current (HVDC) tie-line is modeled to transfer PV generation to load centers. In the meantime, it provides frequency support. Multi-machine system frequency response model is employed to approximate the frequency behaviors. The PV is considered semi-controllable in the scheduling model. A novel solution approach is proposed to solve the unit commitment problem with nonlinear frequency stability constraints. Case studies demonstrate the benefits and effectiveness of the proposed approach.

Keywords: Unit Commitment, semi-dispatchable PV generation, Frequency Stability, HVDC

1. Introduction

The renewable installation capacity has seen a significant increase globally in the last decades, amounting to 3,064 GW [1]. According to International Energy Agency, annual renewable capacity addition reaches almost 295 GW in 2021, and PV growth contributes half of it [2]. In the meantime, utility-scale renewable resources are located in rural areas. HVDC transmission systems are often used to transfer energy in long distances [3]. The rapid development of renewable poses new challenges in power system operation and stability.

The renewables, such as PV and wind, are intermittent and variable resources. When renewable penetration reaches a certain level, the system has to preserve enough reserve to offset the uncertainty stemming from renewable generation. The traditional Unit Commitment (UC) problem determines on/off states of units, which meet load demand and reserve requirement in a cost-efficient fashion [4–6]. There is rich literature on UC with tertiary reserves. Stochastic, robust, and data-driven approaches are successfully employed to optimize reserves for uncertainty management. Among them, scenario-based UC often models the sampling scenarios for renewable output based on some probability distributions [7, 8]. Robust UC guarantees the system has enough reserves to survive in all possible fluctuations stemming from renewable generation [9–11]. Data-driven UC relies on historical data instead of the probability distribution, and immunizes the scheduling against the worst-case distribution in ambiguity set [12].

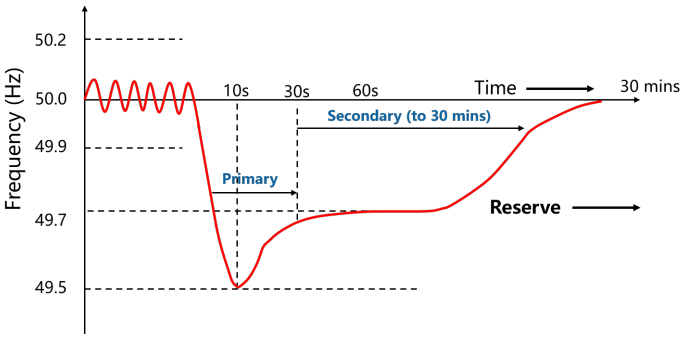

Figure 1: An illustrative figure of frequency control.

Power electronics are widely used in renewable units and HVDC transmission systems. They could lower the system inertia, which is fundamentally important to system stability [13]. Traditional reserve constraints often require more units

Nomenclature

Indices

i	index of thermal units
j	index of partitions of feasible region
t	index of time intervals

Parameters

$\beta^C/\beta^H/\beta^F/\beta^R$	Coefficients of the piecewise linear constraints
$\Delta\overline{R}^{dc}/\Delta\underline{R}^{dc}$	Hourly ramp up/down limit of the HVDC
$\overline{P}^{dc}/\underline{P}^{dc}$	Maximum/minimum power output of the HVDC
$\overline{P}^{dis,dc}/\underline{P}^{dis,dc}$	Largest power disturbance in the receiving end
$\overline{P}_t^{pv}/\underline{P}_t^{pv}$	Maximum/minimum power output of confidence interval of the PV station
$H_i/F_i/R_i/R^{dc}$	Inertia constant/ Fraction of power generated by the high-pressure turbine/ Governor regulation constant of the thermal generator/ HVDC
$RoCoF^{max}$	Maximal rate-of-change of Frequency
S^{dc}	the capacity of HVDC
Δ_t	Downward disturbance requirement
$\overline{P}_i^G/\underline{P}_i^G$	Maximum/minimum power output of the thermal generator
$C_i^P/C_i^R/\mathcal{U}_t^{PV}$	The cost function for UC and Dispatch/ Regulating reserves/ upper and lower bounds for PV output deviation
$f_0/\overline{f}/\underline{f}$	Nominal Frequency/ Frequency zenith/ nadir
$P_t^{D,s}/P_t^{D,r}$	Load demand at sending/receiving end grid
$P_t^{pv,f}$	Forecasted PV output
$P_t^{pv,s}$	Scheduled PV generation
R_g^{UP}/R_g^{DN}	Hourly ramp up/down capacity of the thermal generator
$S_g/S_{sys}^s/S_{sys}^r$	Rated apparent power of the generator/ the sum of the system installed generation capacity in sending/ receiving end
T_g^{on}/T_g^{off}	Minimum online/offline time of the thermal generator

Variables

η_t^s/η_t^r	Auxiliary variable in the sending/receiving end
γ_t^-	Permissible downward deviation for PV generation
$H_t/F_t/R_t$	System aggregated inertia constant/turbine parameter/ governor regulation constant
$I_{i,t}$	Binary variable representing unit i on/off status at time t
$P_{i,t}^G/P_t^{dc}$	Power output of the thermal generator/ HVDC
$P_t^{dis,-}/P_t^{dis,+}$	Permissible deviations of power
$R_{i,t}^{reg,up}/R_{i,t}^{reg,down}$	upward/downward regulating reserve of unit i
$U_{i,t}/V_{i,t}$	Binary variable representing the start up/shut down for unit i
$x_{i,t}$	Binary variable representing whether unit i participating in frequency regulation at time t

online, leading to large system inertia. However, reserves in traditional UC mostly are prepared for secondary and tertiary control. The frequency dynamics are not explicitly modeled [4]. Figure 1 illustrates the frequency control dynamics. With

increasing power electronic enabled assets in power grids, UC considering frequency stability becomes an emerging topic, and attracts great attention in recent years [14–18]. Frequency stability is referred to the ability to maintain steady frequency following a significant imbalance between generation and load [19].

Although there is a rich literature on load-frequency control, it remains an open question to consider frequency dynamics in UC. System transients often involve differential-algebraic equations (DAE) and control strategies, which are challenging to directly address with optimization theories. Researchers put much effort into modeling frequency stability from different perspectives [17, 20, 21]. Most techniques handling frequency limit in UC can be classified into two groups. One is to use the ramp limit to express the loss of kinetic energy so that the frequency limit can be modeled [21, 22]. It avoids the complicated frequency dynamics at the cost of ignoring the control strategies of generators. The other technique is to use the system frequency response (SFR) model to enforce the constraints with the closed form of frequency limit [23]. In [17], the authors employ piecewise hyperplanes to approximate the Multi-machine System Frequency Response (MM-SFR) model in the UC problem. Recently, frequency support from renewables are considered in low-inertia systems [16, 24]. Frequency nadir is often approximated by a nonlinear function in system inertia, turbine parameter, and governor regulation. Additional binary variables are introduced to model the nadir limit. However, it is computationally intensive [17, 24]. Authors in [16] enforce all constraints and disregard piece segments to avoid binary variables, at the cost of over-conservativeness.

In the frequency literature, the disturbance is often modeled as the largest online unit's capacity. However, PV generation could fluctuate significantly due to the nature of solar radiation. We propose an approach to UC and renewable scheduling with frequency limit constraints. The contribution of this work is three-fold.

- We consider the PV generators semi-dispatchable, i.e. their output can be lowered by curtailing renewable energy. It provides additional flexibility in both power balance and frequency stability. The model optimally determines the scheduled PV output and online states for traditional units.
- The HVDC line is modeled to participate in the frequency regulation. There is limited work reporting HVDC line frequency support in UC literature. By modeling the HVDC line response, we can employ inter-regional resources to meet the frequency limit constraints.
- We propose a successive constraint generation (SCG) approach to handling piecewise linear frequency constraints. Different from most techniques in literature, SCG does not employ binary variables or model all constraints. Instead, it iteratively adds newly generated limited constraints until convergence. The simulation results indicate it is computationally efficient yet accurate.

The remainder of this paper is organized as follows. Section II presents the proposed inter-regional UC and renewable scheduling model with frequency nadir limit. Section III proposes a solution approach to the model. The frequency nadir limit constraint is first linearized, and then a successive constraint generation algorithm is presented to solve the problem. We conduct case studies demonstrating the effectiveness of the proposed model and solution approach in section V. Section VI concludes the paper.

2. Model Formulation

Following a generator trip or sudden decrease in PV output, the system frequency continues to drop before exceeding the dead band, and then the primary control kicks in. In a single-machine system, the swing equation describes small deviations around the nominal frequency

$$2H\frac{d\Delta f(t)}{dt} = P_m(t) - P_e(t) = \Delta P_m(t) - \Delta P_e(t), \qquad (1)$$

where $\Delta f(t)$ is the frequency deviation, i.e. $\Delta f(t) = f(t) - f_{nom}$. $P_m(t)$ is the mechanical power, and $P_e(t)$ is the electrical

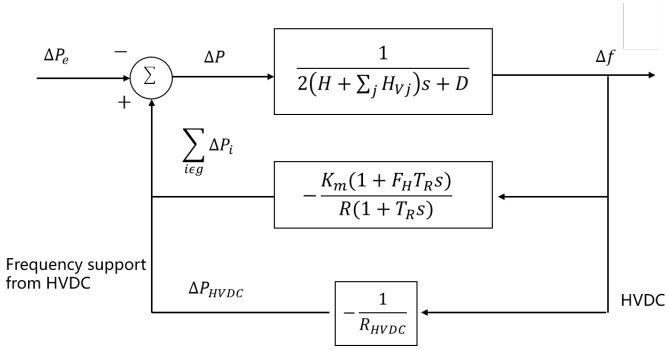

Figure 2: System Frequency Response Model with HVDC Frequency Support.

power. Note $P_e(t)$ consists of frequency-sensitive load and non-frequency-sensitive load. H is the inertia constant [13]. Readers are referred to Figure 1 for the illustrative process. With primary control, the system frequency reaches the nadir point f_{nadir}, and then gets to a new steady state. The new frequency has a deviation from the nominal frequency. If the system is stable, the deviation will be eliminated by automatic generation control (AGC), which gives new setpoints for units. In this section, we present a model capturing the frequency nadir point with frequency support from synchronous generators and HVDC line.

2.1. System Frequency Response

In the power literature, system frequency response (SFR) is often used to approximate the frequency behaviors following a disturbance [23, 25]. We consider the HVDC line can provide frequency support [26]. The transfer function is presented in Figure 2. Following [23, 25], the frequency deviation in the time domain is given as

$$\Delta f(t) = \frac{R\Delta P}{DR+1} \cdot \left[1 + \alpha e^{-\zeta\omega_n t} \sin(\omega_r t + \varphi)\right] \tag{2}$$

where ΔP is defined as the power disturbance. R is the droop parameter, and D is the load-damping constant. In (2), ω_n, ζ, ω_r, α, and ϕ are defined as

$$\begin{cases} \omega_n^2 = \frac{DR+1}{2HRT_R} \\ \zeta = \frac{DRT_R+2HR+F_H T_R}{2(DR+1)}\omega_n \\ \omega_r = \omega_n\sqrt{1-\zeta^2} \\ \alpha = \sqrt{\frac{1-2T_R\zeta\omega_n+T_R^2\omega_R^2}{1-\zeta^2}} \\ \varphi = \arctan\left(\frac{\omega_r T_R}{1-\zeta\omega_n T_R}\right) - \arctan\left(\frac{\sqrt{1-\zeta^2}}{-\zeta}\right) \end{cases} \tag{3}$$

where T_R is the reheat time constant, and F_H is the fraction of total power generated by the high-pressure turbine. As shown in Figure 1, f_{nadir} is reached when $\Delta f(t)' = 0$. With (2), solving $\Delta f(t)' = 0$ gives

$$t_{nadir} = \frac{1}{\omega_r}\arctan\left(\frac{\omega_r T_R}{\zeta\omega_r T_R - 1}\right). \tag{4}$$

Therefore, we have

$$\begin{cases} \Delta f_{nadir} = \Delta P \frac{1+\sqrt{1-\zeta^2}\alpha e^{-\zeta\omega_n t_{nadir}}}{D+1/R} \\ f_{nadir} = f_0 - \Delta f_{nadir}. \end{cases} \tag{5}$$

By introducing an auxiliary function

$$\eta \triangleq \frac{D+1/R}{1+\sqrt{1-\zeta^2}\alpha e^{-\zeta\omega_n t_{nadir}}}, \tag{6}$$

we rewrite equation (5) as

$$P_t^{dis} = (f - f_0)\eta. \tag{7}$$

P_t^{dis} can be upward and downward. It is thus written as

$$\begin{cases} P_t^{dis} = P_t^{dis,+} - P_t^{dis,-} \\ P_t^{dis,+} \geq 0, \quad P_t^{dis,-} \geq 0 \end{cases} \tag{8}$$

2.2. Thermal Unit Constraint

The generator dispatch respects its lower and upper limits. It is formulated as

$$I_{i,t}\underline{P}_i^G \leq P_{i,t}^G \leq I_{i,t}\overline{P}_i^G, \forall t, \forall i, \tag{9}$$

where $I_{i,t}$ is the binary variable indicating if generator i is online or offline at time t. A group of constraints for unit operation is formulated as

$$U_{i,t} - V_{i,t} = I_{i,t} - I_{i,t-1}, \forall t, \forall i \tag{10}$$

$$P_{i,t}^G - P_{i,t-1}^G \leq I_{i,t-1}R_i^{UP} + U_{i,t}\underline{P}_i^G, \forall t, \forall i \tag{11}$$

$$P_{i,t-1}^G - P_{i,t}^G \leq I_{i,t-1}R_i^{DN} + V_{i,t}\underline{P}_i^G, \forall t, \forall i \tag{12}$$

$$\sum_{\tau=t-T_i^{on}-1}^{t-1} I_{i,\tau} \geq V_{i,t}T_i^{on}, \forall t, \forall i \tag{13}$$

$$\sum_{\tau=t-T_i^{off}-1}^{t-1} (1 - I_{i,\tau}) \geq U_{i,t}T_i^{off}, \forall t, \forall i. \tag{14}$$

Let $x_{i,t}$ be the indicator of if unit i participating in frequency regulation. The unit must be online to provide the frequency support, hence

$$x_{i,t} \leq I_{i,t}, \forall i, t. \tag{15}$$

After reaching the steady state, the unit i picks up power is $\Delta P_{i,t} = -S_i/R_i \cdot \Delta f \cdot x_{i,t}$. Therefore, the regulating reserve of unit i can be defined as

$$R_{i,t}^{reg,up} = \frac{S_i}{R_i} \cdot (f_0 - \underline{f}) \cdot x_{i,t}, \forall i, t \tag{16}$$

$$R_{i,t}^{reg,down} = \frac{S_i}{R_i} \cdot (\bar{f} - f_0) \cdot x_{i,t}, \forall i, t \tag{17}$$

where $\bar{f}$ and $\underline{f}$ are upper and lower limits of frequency, respectively. In the meantime, the dispatch should not exceed the unit's output limit

$$P_{i,t}^G + R_{i,t}^{reg,up} \leq \bar{P}_i^G, \forall t, i \in \mathcal{G}_s \tag{18}$$

$$P_{i,t}^G - R_{i,t}^{reg,down} \geq \underline{P}_i^G x_{i,t}, \forall t, i \in \mathcal{G}_s. \tag{19}$$

2.3. PV Generation Constraint

Let $P_t^{pv,f}$ denote the forecast of PV generation. Denote $\underline{P}_t^{pv}$ and $\bar{P}_t^{pv}$ as lower and upper bounds of PV generation confidence interval respectively. Then, the scheduled PV output respects

$$\underline{P}_t^{pv} \leq P_t^{pv,s} \leq P_t^{pv,f}, \forall t. \tag{20}$$

Let Δ_t denote the downward disturbance requirement.

$$\gamma_t^- = P_t^{dis,-} - \Delta_t, \gamma_t^- \geq 0, \forall t \tag{21}$$

Equation (21) denotes permissible downward disturbance is not less than Δ_t, and γ_t^- is the permissible downward deviation for PV generation. Equation (22)-(23) shows the permissible deviations are within the confidence interval of PV generation.

$$\gamma_t^- \leq P_t^{pv,s} - \underline{P}_t^{pv} \tag{22}$$

$$P_t^{dis,+} \leq \bar{P}_t^{pv} - P_t^{pv,s}. \tag{23}$$

2.4. Two-area HVDC System Constraint

The ramp limit of the HVDC tie-line output is modeled in (24).

$$\Delta \underline{R}^{dc} \leq P_t^{dc} - P_{t-1}^{dc} \leq \Delta \overline{R}^{dc}, \forall t \tag{24}$$

The power balance constraint in the sending end grid is formulated in (25).

$$P_t^{pv,s} + \sum_{i \in \mathcal{G}_s} P_{i,t}^G - P_t^{D,s} = P_t^{dc}, \forall t, \forall i \tag{25}$$

The power balance constraint in the receiving end grid is formulated as

$$P_t^{dc} + \sum_{i \in \mathcal{G}_r} P_{i,t}^G = P_t^{D,r}, \forall t, \forall i \tag{26}$$

The largest power disturbance reflected in the receiving end is formulated as

$$\underline{P}_t^{dis,dc} = \frac{S^{dc}}{R^{dc}}(\underline{f} - f_0) \tag{27}$$

$$\bar{P}_t^{dis,dc} = \frac{S^{dc}}{R^{dc}}(\bar{f} - f_0). \tag{28}$$

The HVDC should also keep enough reserves, which are formulated in the equations below.

$$\underline{P}^{dc} - P_t^{dc} \leq \underline{P}_t^{dis,dc}, \forall t \tag{29}$$

$$\bar{P}^{dc} - P_t^{dc} \geq \bar{P}_t^{dis,dc}, \forall t. \tag{30}$$

Therefore, reserves the receiving end grid keeps should not be less than the above values. The network constraints can be also enforced in both sides.

2.5. Frequency Constraint

We employ the aggregated MM-SFR model to derive the frequency limit constraint [25]. Most equations apply in both sending and receiving end grids. For notation simplification, we slightly abuse the superscript s and r. When there is a disturbance, the initial Rate-of-Change-of-Frequency (RoCoF) is a function of the system inertia. Equation (1) describes individual machine dynamics. It is reasonable to use an equivalent unit that reflects the average behaviors of all online generators. The equivalent generator is called the center of inertia (COI) [27]. The unit inertia is converted as

$$H_{i,t}^{sys} = H_i \cdot (S_i/S_{sys}) \cdot x_{i,t}, \tag{31}$$

where S_i is the rated capacity of unit i, and S_{sys} is the system base. Following [27], this paper selects the load demand as S_{sys}, and the inertia constant H_t is given as follows

$$H_t = \sum_i H_{i,t}^{sys}. \tag{32}$$

Therefore, following (1), we can easily get the initial RoCoF and its limit

$$RoCoF = \frac{\Delta f(t)}{\Delta t} = \frac{P_t^{dis}}{2H_t} \leq RoCoF^{max}, \forall t. \tag{33}$$

It is reformulated in linear form as

$$P_t^{dis,-} \le 2RoCoF^{max} \cdot H_t, \forall t. \tag{34}$$

If RoCof exceeds its limit, it may trigger a RoCoF relay.

The power upset cannot exceeds the total available regulating reserve

$$\sum_{i\in\mathcal{G}_s} R_{i,t}^{reg,down} \ge P_t^{dis,+}, P_t^{dis,-} \le \sum_{i\in\mathcal{G}_s} R_{i,t}^{reg,up}, \forall t. \tag{35}$$

In the receiving end, we have

$$\underline{P}_t^{dis,dc} \ge -\sum_{i\in\mathcal{G}_r} R_{i,t}^{reg,up}, \forall t \tag{36}$$

$$\bar{P}_t^{dis,dc} \le \sum_{i\in\mathcal{G}_r} R_{i,t}^{reg,down}, \forall t. \tag{37}$$

To formulate the frequency nadir and zenith limits, we employ the aggregated MM-SFR model introduced in [25]. First, the aggregated parameters can be obtained as

$$\frac{1}{R_t} = \sum_{i\in\mathcal{G}_s} (\frac{S_i}{S_{sys}}) \frac{1}{R_i} x_{i,t} + \frac{S_{dc}}{S_{sys}} \frac{1}{R_{dc}}, \forall t \tag{38}$$

$$H_t = \sum_{i\in\mathcal{G}} H_{i,t}^{sys} + H_{dc}, \forall t \tag{39}$$

$$F_t = \sum_{i\in\mathcal{G}} \lambda_{i,t} F_i x_{i,t} \forall t, \tag{40}$$

where $\lambda_{i,t}$ is defined as

$$\lambda_{i,t} = \frac{(\frac{S_i}{S_{sys}})\frac{1}{R_i}}{\sum_{i\in\mathcal{G}} \left(\frac{S_i}{S_{sys}} \frac{1}{R_i} x_{i,t}\right)} = (\frac{S_i}{S_{sys}}) \frac{R_t}{R_i}, \forall i. \tag{41}$$

It is observed that $\lambda_{i,t}$ is a function of $\{x_{i,t}\}$. Therefore, the frequency nadir and zenith constraints are formulated as

$$(\underline{f} - f_0)\eta_t^s S_{sys}^s \le P_t^{dis} \le (\bar{f} - f_0)\eta_t^s S_{sys}^s, \tag{42}$$

where η_t^s is a nonlinear function of (R_t, H_t, F_t).

Similarly, we can establish the frequency constraints for the receiving end grid

$$(\bar{f} - f_0)\eta_t^r S_{sys}^r \ge \bar{P}_t^{dis,dc} \tag{43}$$

$$(f_0 - \underline{f})\eta_t^r S_{sys}^r \ge -\underline{P}_t^{dis,dc}. \tag{44}$$

The power disturbance propagates to the receiving end in several seconds. Hence, the above constraints are conservative. Substitute $\bar{P}_t^{dis,dc}$ and $\underline{P}_t^{dis,dc}$ with (27) and (28), respectively, (43-44) are equivalent to

$$\eta_t^r \ge \frac{S^{dc}}{S_{sys}^r R^{dc}}. \tag{45}$$

2.6. Optimization Model

The frequency-constrained UC problem is formulated as

$$\begin{aligned}(\mathrm{P}) \quad \min \quad & \sum_{t\in\mathcal{T}} \sum_{i\in\mathcal{G}_s\cup\mathcal{G}_r} C_i^P(U_{i,t}, V_{i,t}, P_{i,t}) + C_i^R(R_{i,t}^{reg,down}, R_{i,t}^{reg,up}) \\ & - \sum_{t\in\mathcal{T}} \mathcal{U}_t^{PV}(\gamma_t^- + P_t^{dis,+}) \\ \text{s.t.} \quad & (8-30), (34-42), (45)\end{aligned}$$

where $C_i^P(\cdot)$ denotes the cost function for UC and dispatch, and $C_i^R(\cdot)$ represents the cost function for the regulating reserves. $\mathcal{U}_t(\cdot)$ is the utility function of the upper and lower bounds for PV output deviation.

3. Solution Approach

In the proposed model (P), the frequency limit constraint (42)- (44) are nonlinear and nonconvex. UC problem itself is computationally intensive for utility-scale power systems. The nonlinear term η_t^r and η_t^s make it even more challenging. In this section, we propose a solution approach to reducing the computation burden.

3.1. Linearization

First, we linearize η_t^s, which is a function of parameter R_t^s, H_t^s and F_t^s. Piecewise linearization techniques are often employed to linearize it [16, 24]. According to (40), $\frac{F_t}{R_t}$ is linear in binary variable $\{x_{i,t}\}$. Hence, we employ a linear function of $\{H_t, \frac{1}{R_t}, \frac{F_t}{R_t}\}$ to approximate η_t.

Let $X_t = \{H_t, \frac{1}{R_t}, \frac{F_t}{R_t}\}$, and $\mathcal{X}_t = \{X_t | (38) - (40)\}$ be the feasible region of η_t. Partition $\mathcal{X}_t$ to J parts,

$$\mathcal{X}_t = \cup_{j=1}^J \mathcal{X}_{t,j}. \tag{46}$$

Let $\tilde{\eta}_{t,j}$ represent the hyperplane to approximate η_t in region $\mathcal{X}_{t,j}$. We have

$$\tilde{\eta}_{t,j} \triangleq \beta_j^C + \beta_j^H H_t + \beta_j^F \frac{F_t}{R_t} + \beta_j^R \frac{1}{R_t}, \tag{47}$$

$$= \beta_j^C + \beta_j^H H_t + \beta_j^F \sum_{i\in\mathcal{G}_s} \frac{F_i}{\hat{R}_i} x_{i,t} + \beta_j^R \sum_{i\in\mathcal{G}_s} \frac{1}{\hat{R}_i} x_{i,t}, \tag{48}$$

where $\beta_j^{(\cdot)}$ are parameters to be determined, and $\hat{R}_i = \frac{S_{sys}}{S_i} R_i$. Substituting (38)-(40) to (47) gives (48). By generating a set of

samples, one can use a closed form or supporting vector to get these parameters. Constraint (42) can be approximated by

$$(\underline{f} - f_0)\tilde{\eta}^s_{t,j} S^s_{sys} \le P^{dis}_t \le (\bar{f} - f_0)\tilde{\eta}^s_{t,j} S^s_{sys}, \forall t, \text{ if } X_t \in \mathcal{X}_{t,j}. \quad (49)$$

Similarly, (45) is approximated by

$$\tilde{\eta}^r_{t,j} \ge \frac{S^{dc}}{S^r_{sys} R^{dc}}, \forall t, \text{ if } X_t \in \mathcal{X}_{t,j}. \quad (50)$$

3.2. Successive Constraint Generation Algorithm

In this subsection, we present a successive constraint generation algorithm to solve the frequency-constrained UC problem. First, we replace the nonlinear constraints in (P) with piecewise ones, and establish a UC model as the following.

$$\begin{aligned}(\text{P1}) \quad \min \quad & \sum_{t\in\mathcal{T}} \sum_{i\in\mathcal{G}_s\cup\mathcal{G}_r} C^P_i(U_{i,t}, V_{i,t}, P_{i,t}) + C^R_i(R^{reg,down}_{i,t}, R^{reg,up}_{i,t}) \\ & - \sum_{t\in\mathcal{T}} \mathcal{U}^{PV}_t(\gamma^-_t + P^{dis,+}_t) \\ \text{s.t.} \quad & (21), (8-30), (34-37), (47-50).\end{aligned}$$

Note $\tilde{\eta}_{t,j}$ in constraint (49) and (50) is a function of $\{x_{i,t}\}$. One can introduce a binary variable to indicate whether X_t is within $\mathcal{X}_{t,j}$. It is computationally intensive when the partition or constraint number grows.

At the optimal point, X_t falls only in one partition. However, it is unknown before solving the problem. We introduce a successive algorithm to generate constraints. Let $\mathcal{J}^1_t, \mathcal{J}^2_t$, and $\mathcal{J}^3_t$ be the constraint sets. A master problem (MP) is established as follows

$$\begin{aligned}(\text{MP}) \quad \min \quad & \sum_{t\in\mathcal{T}} \sum_{i\in\mathcal{G}_s\cup\mathcal{G}_r} C^P_i(U_{i,t}, V_{i,t}, P_{i,t}) + C^R_i(R^{reg,down}_{i,t}, R^{reg,up}_{i,t}) \\ & - \sum_{t\in\mathcal{T}} \mathcal{U}^{PV}_t(\gamma^-_t + P^{dis,+}_t) \\ \text{s.t.} \quad & (21), (8-30), (34-37), (47) \\ & (\underline{f} - f_0)\tilde{\eta}^s_{t,j} + P^{dis,-}_t \le 0, \forall t, j \in \mathcal{J}_1 \quad (51) \\ & P^{dis,+}_t - (\bar{f} - f_0)\tilde{\eta}^s_{t,j} \le 0, \forall t, j \in \mathcal{J}_2 \quad (52) \\ & \tilde{\eta}^r_{t,j} \ge \frac{S^{dc}}{R^{dc}}, \forall t, j \in \mathcal{J}_3. \quad (53)\end{aligned}$$

Let k be the number of frequency violation constraints. Algorithm 1 presents the proposed pseudo code of the proposed SCG algorithm. In each iteration, the violated frequency constraints are added cumulatively. When the procedure is converged, we get the UC solution without any frequency constraint violations.

Algorithm 1 Successive Constraint Generation

```
Set J_t^1 = J_t^2 = J_t^3 = ∅
Initialize k, set tolerance δ
while k ≠ 0 do
    Solve (MP), get {x*_{i,t}}
    k ← 0
    for t = 1 : T do
        Get {X_t} according to (38-40) with {x*_{i,t}}
        Determine j, so that X_t ∈ X_{t,j}
        Get η̃_{t,j} according to (47)
        if (f − f_0)η̃^s_{t,j} + P^{dis,−}_t ≥ δ then
            J_t^1 ← J_t^1 ∪ j, k ← k + 1
        else if P^{dis,+}_t − (f̄ − f_0)η̃^s_{t,j} ≥ δ then
            J_t^2 ← J_t^2 ∪ j, k ← k + 1
        end if
        if η̃^{r,eq}_{t,j} − S^{dc}/R^{dc} ≤ δ then
            J_t^3 ← J_t^3 ∪ j, k ← k + 1
        end if
    end for
end while
```

4. Case Study

In this section, we conduct case studies with a modified IEEE RTS-79 system. The HVDC tie-line connects Bus 6 and Bus 23. The sending end grid consists of seven buses from Bus 15 to Bus 23. The PV farm has an installed capacity of 600 MW. There are 11 generators in the sending-end grid. In the receiving end grid, there is a peak load of 957 MW. Table 1 lists generator parameters for traditional UC. The frequency response parameters of thermal generators and HVDC are presented in Table 2. Table 3 lists the unit types of all generators. Δ_t is set to 90 MW. The simulations are carried out on a laptop with AMD R5 3550H 2.1 GHz and the optimization problem is

Table 1: Parameters of the thermal generators

Generation type	U155	U350	U76	U197
Capacity (MW)	155	350	76	197
Variable cost ($/MW)	30	20	45	35
Start-up cost ($/MW)	2	4	6	6
Shut-down cost ($/MW)	2	4	6	6
Min. on time (h)	8	8	4	4
Min. off time (h)	8	8	4	4
Ramp limit	10%	10%	10%	20%
Min. output	35%	50%	20%	20%

Table 2: Frequency response characteristics of thermal generators and HVDC

Gen Type	U155	U350	U76	U197	HVDC
Inertia constant (s)	6	8	4	6	4
Turb. factor F_H	0.3	0.35	0.25	0.3	-
Droop factor	0.05	0.05	0.033	0.033	0.045

solved with Gurobi 9.5.

4.1. Impact of Frequency Constraints

Enforcing frequency constraints can change the UC results. The fuel cost increases from $579,800 to $662,900 due to the frequency constraints. Figure 3 depicts the UC results in the sending end grid without frequency constraints, and Figure 4 shows that with frequency constraints. The x-axis is the time interval and the y-axis denotes the unit index. The background color shows if the unit is committed. The blue cell denotes

Table 3: Unit Type in The Modified IEEE RTS-79 System

Unit No	U155	U350	U76	U197
1-3 (Sending End)	-	-	x	-
4-6 (Sending End)	x	-	-	-
7-8 (Sending End)	-	-	-	x
9-11 (Sending End)	-	x	-	-
1 (Receiving End)	-	x	-	-
2 (Receiving End)	-	-	x	-
3-4 (Receiving End)	x	-	-	-
5-7 (Receiving End)	-	-	-	x

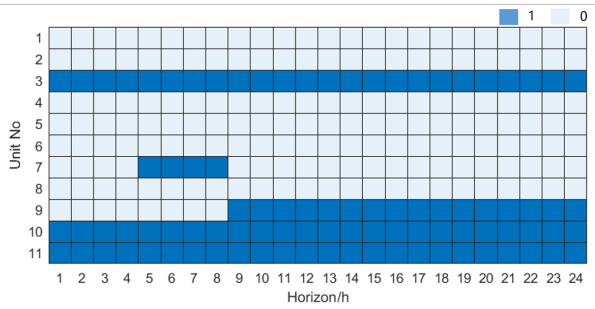

Figure 3: UC results without frequency constraints in the sending end grid

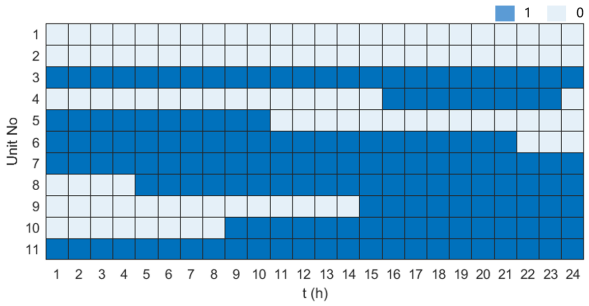

Figure 4: UC results with frequency constraints in the sending end grid

the unit is online, i.e. committed. Committed hours of Unit 3 and 11 remain the same in both cases. Enforcing frequency constraints leads to more committed hours of Unit 1, 2, 5, 7, and 8 commit and fewer committed hours of Unit 10. For example, Unit 1, 2, 5, and 8 are not committed across all time intervals. After enforcing frequency constraints, Unit 8 is committed from Hour 5 to Hour 9. Similarly, Unit 5 is committed from Hour 1 to Hour 8 when frequency constraints are enforced. In contrast, Unit 10 is turned off from Hour 1 to Hour 8. It is observed that the frequency constraints in general require more committed units. That is because more online units often indicate larger system inertia, which is relevant to frequency regulation capability.

4.2. Impact of HVDC Frequency Support

The HVDC tie-line provides frequency support by mitigating the power disturbance in the sending end grid. Figure 5 presents the comparison of permissible downward disturbances. The blue dashed dot line is the permissible disturbance without HVDC frequency support, and the orange dashed line presents that with HVDC frequency support. It can be observed that the

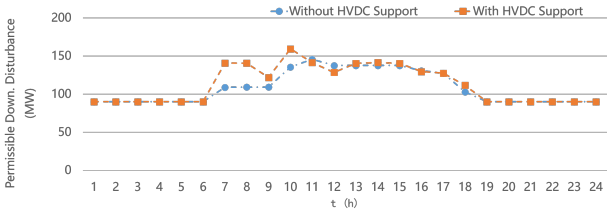

Figure 5: Permissible downward disturbance with and without HVDC frequency support

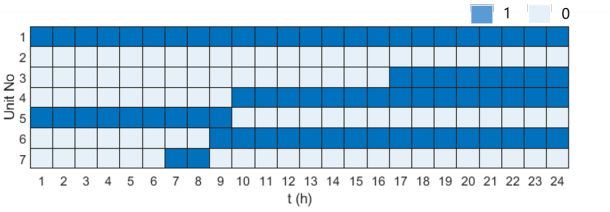

Figure 6: $x_{i,t}$ with HVDC frequency support in the receiving end grid. $x_{i,t} = 1$ indicates participating frequency regulation.

frequency support from HVDC helps increase the permissible power disturbance. For example, the original max permissible disturbance is 135 MW, which is attained at Hour 11. With HVDC frequency support, the max permissible disturbance increases to 159 MW at Hour 10. Also, together with Figure 4, we observe that permissible disturbance increases with online capacity. Figure 5 shows the largest permissible disturbance achieved at Hour 10 when there is a large online capacity according to Figure 4.

The HVDC tie-line helps utilize the inter-regional resources to regulate the frequency. Adding HVDC frequency support lowers the objective from 574,100 to 567,400. Figure 6 shows the generators participating in frequency support in the receiving end grid. It is observed that Unit 5 and 7 of type U197 involves the frequency regulation at Hour 7 and 8 when the system has a high permissible downward disturbance. In contrast, Unit 5 does not provide frequency regulation if HVDC frequency support is not added. It indicates that units in the receiving end grid are indirectly utilized when HVDC participates in the frequency regulation. The disturbances propagate to the receiving end grid according to equation (27-28).

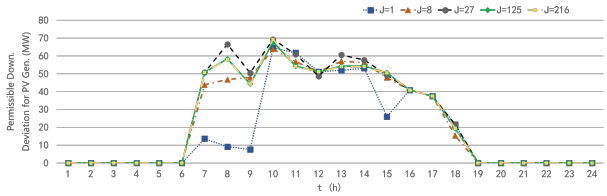

Figure 7: Different frequency-secure downward deviations attained by the proposed SCG with various pieces.

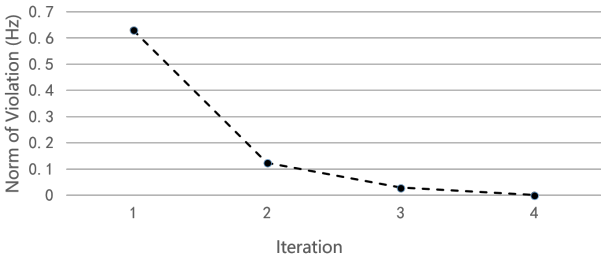

Figure 8: Various frequency nadirs with iterations in SCG algorithm

4.3. Performance of Proposed SCG Algorithm

In this part, we conduct simulations to verify the performance of the proposed SCG algorithm. Figure 7 draws the different frequency-secure downward deviations for PV generation attained by SCG when various piece numbers are used. $J = 1$ indicates only one piece is used, and it has small values from Hour 6 to Hour 9. We observe that curves are close after $J \geq 27$. For example, the curve of $J = 125$ almost overlaps with that of $J = 216$. It shows the convergence of the approximation accuracy. It indicates that the nonlinear frequency constraints are accurately approximated with the proposed approach.

Figure 8 shows frequency violations with iterations in the proposed SCG algorithm. It is observed that the procedure converges after four iterations in this case. According to our experiments, the SCG algorithm converges within four or three iterations.

For the convenience of comparison, we call the technique used in [16] one-shot linearization (OSL). Figure 9 shows the comparison of permissible downward deviation for PV generation attained by OSL and SCG. The blue dashed dot is calculated based on OSL, and the orange dashed line is attained from the proposed SCG algorithm. It can be observed that the

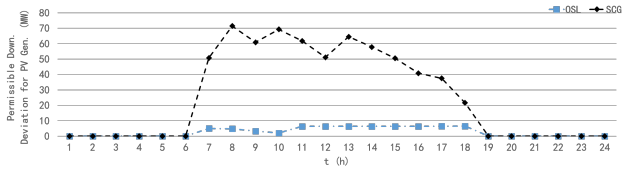

Figure 9: Frequency-secure downward deviation for PV generation from the proposed SCG and OSL algorithm.

Table 4: Model and Performance Comparison

	Constraint #	Obj. Value	Solution Time (s)
OSL	10,363	589,000	32.8
SCG	4,411	579,500	23.0

frequency-secure deviation obtained from the SCG algorithm is much larger than that attained from OSL. For example, the frequency-secure deviation by OSL is below 10 MW from Hour 7 to Hour 18. In contrast, the frequency-secure deviation by the proposed SCG ranges from 21 MW to 70 MW from Hour 7 to Hour 18. That is because the feasible region in OSL is conservatively shrunk when modeling frequency constraints. It indicates that the proposed SCG could safely integrate more solar energy if PV generation suddenly increases.

Table 4 compares the model and computation performance of OSL and the proposed SCG. The column "Constraint #" lists the constraint number of the model. It is observed that the converged model in SCG has 4,429 constraints, which are 5,952 = 10,363 - 4,411 less than that in OSL. In the meantime, the objective value is listed in column "Obj. Value" from SCG is $579,500, which is $ 9,500 = 589,000-579,500 less than that from OSL. It indicates the shrunk feasible region in OSL leads to a conservative result. The column "Solution Time (s)" lists the total solution time. SCG takes 23.0 s to find the solution while OSL needs 32.8 s . It indicates SCG in general is more computationally efficient than OSL.

5. Conclusion

A large-scale renewable integration in the power system may lower the system inertia, which is fundamentally important to frequency security. This work presents a unit commitment model considering HVDC frequency support. Permissible deviation for PV generation is modeled to increase renewable accommodation. A successive constraints generation (SCG) algorithm is proposed to address the nonlinear frequency constraints. The simulation results show that HVDC frequency support can increase the permissible power disturbance, and the proposed algorithm outperforms the existing approach in terms of accuracy and speed.

References

[1] Renewable capacity highlights 2022, Tech. rep., International Renewable Energy Agency (April 2022).

[2] H. Bahar, J. Moorhouse, Renewable Energy Market Update 2022, Tech. rep., International Energy Agency (2022).

[3] J. Sun, M. Li, Z. Zhang, T. Xu, J. He, H. Wang, G. Li, Renewable energy transmission by hvdc across the continent: system challenges and opportunities, CSEE Journal of Power and Energy Systems 3 (4) (2017) 353–364. doi:10.17775/CSEEJPES.2017.01200.

[4] M. Shahidehpour, H. Yamin, Z. Li, Market Operations in Electric Power Systems: Forecasting, Scheduling, and Risk Management, 1st Edition, Wiley-IEEE Press, 2002.

[5] X. Guan, P. Luh, H. Yan, J. Amalfi, An optimization-based method for unit commitment, International Journal of Electrical Power & Energy Systems 14 (1) (1992) 9–17. doi:https://doi.org/10.1016/0142-0615(92)90003-R.

[6] M. Paredes, L. Martins, S. Soares, H. Ye, Benders' decomposition of the unit commitment problem with semidefinite relaxation of ac power flow constraints, Electric Power Systems Research 192 (2021) 106965. doi:https://doi.org/10.1016/j.epsr.2020.106965.

[7] L. Wu, M. Shahidehpour, T. Li, Stochastic Security-Constrained Unit Commitment, IEEE Transactions on Power Systems 22 (2) (2007) 800–811. doi:10.1109/TPWRS.2007.894843.

[8] T. Shiina, J. R. Birge, Stochastic unit commitment problem, International Transactions in Operational Research 11 (1) (2004) 19–32. doi:https://doi.org/10.1111/j.1475-3995.2004.00437.x.

[9] D. Bertsimas, E. Litvinov, X. Sun, J. Zhao, T. Zheng, Adaptive Robust Optimization for the Security Constrained Unit Commitment Problem, IEEE Transactions on Power Systems 28 (1) (2013) 52–63. doi:10.1109/TPWRS.2012.2205021.

[10] R. Jiang, M. Zhang, G. Li, Y. Guan, Two-stage network constrained robust unit commitment problem, European Journal of Operational Research 234 (3) (2014) 751–762.

[11] H. Ye, Z. Li, Robust Security-Constrained Unit Commitment and Dispatch with Recourse Cost Requirement, IEEE Transactions on Power Systems 31 (5) (2016) 3527–3536. doi:10.1109/TPWRS.2015.2493162.

[12] C. Duan, L. Jiang, W. Fang, J. Liu, Data-driven affinely adjustable distributionally robust unit commitment, IEEE Transactions on Power Systems 33 (2) (2018) 1385–1398. doi:10.1109/TPWRS.2017.2741506.

[13] P. Kundur, Power System Stability and Control, McGraw-Hill Professional, 1994.

[14] Y. Wen, W. Li, G. Huang, X. Liu, Frequency Dynamics Constrained Unit Commitment With Battery Energy Storage, IEEE Transactions on Power Systems 31 (6) (2016) 5115–5125. doi:10.1109/TPWRS.2016.2521882.

[15] J. Man, X. Xie, S. Xu, C. Zou, C. Yin, Frequency-Coupling Impedance Model Based Analysis of a High-Frequency Resonance Incident in an Actual MMC-HVDC System, IEEE Transactions on Power Delivery 35 (6) (2020) 2963–2971. doi:10.1109/TPWRD.2020.3022504.

[16] Z. Zhang, E. Du, F. Teng, N. Zhang, C. Kang, Modeling Frequency Dynamics in Unit Commitment With a High Share of Renewable Energy, IEEE Transactions on Power Systems 35 (6) (2020) 4383–4395. doi:10.1109/TPWRS.2020.2996821.

[17] H. Ahmadi, H. Ghasemi, Security-Constrained Unit Commitment With Linearized System Frequency Limit Constraints, IEEE Transactions on Power Systems 29 (4) (2014) 1536–1545. doi:10.1109/TPWRS.2014.2297997.

[18] L. Badesa, F. Teng, G. Strbac, Simultaneous Scheduling of Multiple Frequency Services in Stochastic Unit Commitment, IEEE Transactions on Power Systems 34 (5) (2019) 3858–3868. doi:10.1109/TPWRS.2019.2905037.

[19] P. Kundur, J. Paserba, V. Ajjarapu, G. Andersson, A. Bose, C. Canizares, N. Hatziargyriou, D. Hill, A. Stankovic, C. Taylor, T. Van Cutsem, V. Vittal, Definition and classification of power system stability IEEE/CIGRE joint task force on stability terms and definitions, IEEE Transactions on Power Systems 19 (3) (2004) 1387–1401. doi:10.1109/TPWRS.2004.825981.

[20] X. Lei, E. Lerch, C. Xie, Frequency security constrained short-term unit commitment, Electric Power Systems Research 60 (3) (2002) 193–200. doi:https://doi.org/10.1016/S0378-7796(01)00177-8.

[21] Y.-Y. Lee, R. Baldick, A frequency-constrained stochastic economic dispatch model, IEEE Transactions on Power Systems 28 (3) (2013) 2301–2312. doi:10.1109/TPWRS.2012.2236108.

[22] C. J. Ferrandon-Cervantes, B. Kazemtabrizi, M. C. M. Troffaes, Inclusion of frequency stability constraints in unit commitment using separable programming, Electric Power Systems Research 203 (2022) 107669. doi:10.1016/j.epsr.2021.107669.

[23] P. Anderson, M. Mirheydar, A low-order system frequency response model, IEEE Transactions on Power Systems 5 (3) (1990) 720–729. doi:10.1109/59.65898.

[24] M. Paturet, U. Markovic, S. Delikaraoglou, E. Vrettos, P. Aristidou, G. Hug, Stochastic Unit Commitment in Low-Inertia Grids, IEEE Transactions on Power Systems 35 (5) (2020) 3448–3458. doi:10.1109/TPWRS.2020.2987076.

[25] Q. Shi, F. Li, H. Cui, Analytical Method to Aggregate Multi-Machine SFR Model With Applications in Power System Dynamic Studies, IEEE Transactions on Power Systems 33 (6) (2018) 6355–6367. doi:10.1109/TPWRS.2018.2824823.

[26] L. Fan, Z. Miao, D. Osborn, Wind Farms With HVDC Delivery in Load Frequency Control, IEEE Transactions on Power Systems 24 (4) (2009) 1894–1895. doi:10.1109/TPWRS.2009.2030256.

[27] U. Rudez, R. Mihalic, Monitoring the First Frequency Derivative to Improve Adaptive Underfrequency Load-Shedding Schemes, IEEE Transactions on Power Systems 26 (2) (2011) 839–846. doi:10.1109/TPWRS.2010.2059715.